Three-body breakup of ^{11}Li with the eikonal method

E. C. Pinilla,[1] P. Descouvemont,[1] and D. Baye[1,2]
[1]*Physique Nucléaire Théorique et Physique Mathématique, C.P. 229, Université Libre de Bruxelles (ULB), B 1050 Brussels, Belgium*
[2]*Physique Quantique, C.P. 165/82, Université Libre de Bruxelles (ULB), B 1050 Brussels, Belgium*
(Received 3 April 2012; published 7 May 2012)

The ^{11}Li breakup on a ^{208}Pb target is studied in the Coulomb-corrected eikonal approximation by using a $^{9}\mathrm{Li}+n+n$ three-body description of the projectile. The ^{11}Li wave functions are defined in the hyperspherical formalism for bound and scattering states and are obtained from effective $^{9}\mathrm{Li}+n$ and $n+n$ interactions. We first determine 0^+, 1^-, and 2^+ $^{9}\mathrm{Li}+n+n$ phase shifts, which suggest the existence of a narrow 1^- resonance near 0.5 MeV above threshold. The calculated breakup cross sections show a peak at low energies, in agreement with the data. The influence of monopole and quadrupole components is analyzed and shown to be non-negligible. We discuss the derivation of dipole strengths from experimental breakup cross sections and suggest that the simple Coulomb dipole approximation, traditionally used in the literature, should be replaced by more elaborate models. We also show that $^{11}\mathrm{Li}+{}^{208}$Pb elastic scattering measurements would provide an indirect test of the model.

DOI: 10.1103/PhysRevC.85.054610 PACS number(s): 25.60.Gc, 24.10.−i, 27.20.+n

I. INTRODUCTION

Breakup reactions represent an efficient tool for the experimental investigation of exotic nuclei [1]. In particular, reactions involving a radioactive ^{11}Li beam on various targets have been carried out in recent years (see Ref. [2] and references therein). An accurate theoretical description of the breakup process requires a reaction theory complemented by a precise description of the projectile wave function. At low energies, the continuum discretized coupled channel (CDCC) formalism [3] is known to provide reliable cross sections, not only for elastic scattering, but also for breakup cross sections. At higher energies, that is, much higher than the Coulomb barrier, the number of partial waves in the CDCC approach may become prohibitive. Under those conditions, the eikonal approximation [4–6] is well adapted and simpler than the CDCC theory. As the traditional eikonal is known to diverge for the Coulomb potential, we use here a recent extension, the Coulomb-corrected eikonal method [7–9], which avoids the convergence problem in breakup cross sections.

The second ingredient for the calculation is the projectile wave function. The ^{11}Li nucleus is weakly bound [10] and presents a marked halo structure [11]. Its unusually large rms radius can be well reproduced by three-body models, involving a ^{9}Li core surrounded by two neutrons, forming a halo. In addition to the ground state, 0^+ and 1^- resonances have been predicted by different authors [12–14], but not yet firmly established experimentally.

In the present work, we describe ^{11}Li in the three-body hyperspherical formalism [15,16]. This theoretical framework for the projectile can be implemented in the eikonal theory [17]. The hyperspherical model provides the ^{11}Li ground state, but also $^{9}\mathrm{Li}+n+n$ three-body scattering states [18,19]. This property allows a simultaneous and consistent description of elastic scattering and of breakup reactions.

The goal of the present work is to investigate recent breakup data of ^{11}Li on a ^{208}Pb target at 70 MeV/nucleon [2]. These cross-section data present a maximum near 0.3 MeV above the $^{9}\mathrm{Li}+n+n$ threshold, which could be associated with a dipole resonance in ^{11}Li [20]. The present eikonal model does not make any assumption on the Coulomb or nuclear character of the breakup process. Although dipole transitions are expected to be dominant, other multipoles are included. The ^{11}Li wave functions are expanded over a Lagrange basis [21] which allows simple determinations of the matrix elements. For scattering states, the variational calculation is extended to an R-matrix approach [19,22] which provides continuum wave functions with correct asymptotic behavior. These continuum states are used as final states in the calculation of breakup cross sections.

In the literature, the scattering wave functions are often simplified to approximate square integrable functions, defined at discrete energies. As discussed in Ref. [23], this approach, referred to as the pseudostate method [20], must be complemented by a folding procedure to define a continuous energy dependence of the cross section. This additional smearing introduces some ambiguity through the width of the folding function. The present calculations offers the opportunity to assess this simplified method for ^{11}Li breakup.

Assuming a dipole Coulomb process, the breakup cross section can be expressed in terms of a dipole strength distribution [5]. This approximation provides much simpler calculations because only $E1$ excitations of the projectile are necessary. Dipole distributions have been derived by Nakamura *et al.* [2] from their experimental breakup cross sections and are often used for comparison with the theory [14,20,24]. The present approach makes it possible to compute the $E1$ distribution and the breakup cross section independently.

The paper is organized as follows. In Sec. II, we present a brief outline of the three-body model in the hyperspherical formalism. We emphasize the description of scattering states within the R-matrix theory. Section III is devoted to the calculation of elastic and breakup cross sections at the eikonal approximation. The conditions of the calculations are presented in Sec. IV, and the results are presented in Sec. V. In Sec. VI, we discuss the experimental determination of the $E1$ strength from breakup cross sections. Concluding remarks and an outlook are presented in Sec. VII.

II. THREE-BODY MODEL OF THE PROJECTILE

A. The hyperspherical method

The hyperspherical formalism is an efficient tool that makes it possible to calculate bound and scattering states of Borromean systems. For details, we refer the reader to Refs. [15,16,19,25,26]. Let us formulate the three-body problem of a core + n + n system, with a structureless zero-spin core, in hyperspherical coordinates. We start by defining the set of scaled Jacobi coordinates as

$$\boldsymbol{x} = \frac{1}{\sqrt{2}}(\boldsymbol{r}_3 - \boldsymbol{r}_2), \quad \boldsymbol{y} = \sqrt{\frac{2A_1}{A_1+2}}\left(\boldsymbol{r}_1 - \frac{\boldsymbol{r}_2+\boldsymbol{r}_3}{2}\right), \tag{1}$$

where $\boldsymbol{r}_1$ is the core coordinate with mass A_1 and charge $Z_1 e$, and $\boldsymbol{r}_2$ and $\boldsymbol{r}_3$ are the neutron coordinates, respectively.

For a total angular momentum JM and parity π, we solve the time-independent Schrödinger equation

$$H_{3b}\Psi^{JM\pi} = E\Psi^{JM\pi}, \tag{2}$$

where E is the three-body energy. After removal of the center-of-mass motion, the Hamiltonian is given by

$$H_{3b} = -\frac{\hbar^2}{2m_N}(\Delta_x + \Delta_y) + V_{12} + V_{13} + V_{23}, \tag{3}$$

where V_{12} and V_{13} are effective potentials, usually taken as Woods-Saxon or Gaussian potentials, and V_{23} is a nucleon + nucleon interaction. In Eq. (3), m_N is the nucleon mass.

We solve Eq. (2) by writing the Hamiltonian in terms of hyperspherical coordinates

$$\rho^2 = x^2 + y^2, \quad \alpha = \arctan\frac{y}{x}; \quad 0 \leqslant \alpha \leqslant \frac{\pi}{2}, \tag{4}$$

and by expanding the wave function as

$$\Psi^{JM\pi} = \rho^{-5/2}\sum_{K=0}^{\infty}\sum_{\gamma}\chi^{J\pi}_{\gamma K}(\rho)\mathcal{Y}^{JM}_{\gamma K}(\Omega_{5\rho}). \tag{5}$$

In this definition, index γ represents the set of quantum numbers $\gamma = (l_x, l_y, L, S)$, where L is the total orbital momentum, $S = 0, 1$ is the total intrinsic spin, and l_x and l_y are the orbital momenta associated with $\boldsymbol{x}$ and $\boldsymbol{y}$. In practice, the sum over the hypermomentum K is limited to a maximum value $K_{\max}$, and the parity $\pi = (-1)^K$ of the three-body relative motion restricts the sum to even or odd values. The hyperspherical harmonics $\mathcal{Y}^{JM}_{\gamma K}$ depend on a set of five angles [15] $\Omega_{5\rho} = (\Omega_x, \Omega_y, \alpha)$ and are obtained from the coupling of a space component and of a spin state. The unknown hyper-radial wave functions are denoted as $\chi^{J\pi}_{\gamma K}(\rho)$.

Expansion (5) provides the set of coupled differential equations,

$$\left\{-\frac{\hbar^2}{2m_N}\left[\frac{d^2}{d\rho^2} - \frac{(K+3/2)(K+5/2)}{\rho^2}\right] - E\right\}\chi^{J\pi}_{\gamma K}(\rho) + \sum_{K'\gamma'} V^{J\pi}_{\gamma K,\gamma' K'}(\rho)\,\chi^{J\pi}_{\gamma' K'}(\rho) = 0, \tag{6}$$

where $V^{J\pi}_{\gamma K,\gamma' K'}(\rho)$ stands for the potential matrix elements between hyperspherical harmonics [16]. These potentials are known to behave, at large ρ values, as

$$V^{J\pi}_{\gamma K,\gamma' K'}(\rho) \sim 1/\rho^3, \tag{7}$$

and therefore extend to large distances. This property is important for the treatment of three-body scattering states.

The hyper-radial wave functions are determined with the Lagrange-mesh technique [21,27], which approximately corresponds to a variational treatment on a mesh. In other words, we expand the hyper-radial wave function on N square-integrable basis functions $u_i(\rho)$ as

$$\chi^{J\pi}_{\gamma K}(\rho) = \sum_{i=1}^{N} c^{J\pi}_{\gamma K i}u_i(\rho). \tag{8}$$

A Lagrange basis is a set of indefinitely differentiable orthonormal functions that vanish at all points except one of an associated mesh. The Lagrange-mesh technique leads to simple calculations when the matrix elements are calculated at the Gauss approximation corresponding to the mesh. It provides analytical matrix elements of the kinetic energy and diagonal potential matrix elements obtained by a simple evaluation of the potential at the mesh points. As basis functions $u_i(\rho)$, we choose Lagrange-Legendre functions defined in a finite interval [22]. This basis is used to describe continuum as well as bound states of the system.

B. Scattering states

We wish to find solutions of Eq. (2) for energies $E > 0$ with the correct boundary conditions. A scattering state with outgoing boundary conditions is defined as [26]

$$\Psi^{(+)}_{\boldsymbol{k}_x\boldsymbol{k}_y S\nu}(E, \boldsymbol{k}_x, \boldsymbol{k}_y) = (2\pi)^{-3}\rho^{-5/2}\sum_{JM}\sum_{l'_x l'_y L' K'}(L'SM'_L\nu|JM)\mathcal{Y}^{L'M'_L *}_{l'_x l'_y K'}(\Omega_{5\kappa}) \times \sum_{\gamma K}\mathcal{Y}^{JM}_{\gamma K}(\Omega_{5\rho})\chi^{J\pi}_{\gamma K(\gamma' K')}(E,\rho), \tag{9}$$

where $\hbar k = \hbar\sqrt{k_x^2 + k_y^2} = \sqrt{2m_N E}$ is the hypermomentum, with $\hbar\boldsymbol{k}_x$ and $\hbar\boldsymbol{k}_y$ the canonical conjugate momenta of the Jacobi coordinates $\boldsymbol{x}$ and $\boldsymbol{y}$. Indices $\gamma' K'$ label the entrance channel. Here, we explicitly display the dependence of the scattering wave function with the excitation energy E of the three-body projectile (defined from the three-body threshold).

The hyper-radial wave functions fulfill the boundary conditions $\chi^{J\pi}_{\gamma K(\gamma' K')}(0) = 0$ and, at large distances, tend to

$$\chi^{J\pi}_{\gamma K(\gamma' K')}(E,\rho) \underset{\rho\to\infty}{\longrightarrow} i^{K'+1}(2\pi/k)^{5/2}\left[H^-_{\gamma K}(k\rho)\delta_{\gamma\gamma'}\delta_{KK'} - U^{J\pi}_{\gamma K,\gamma' K'}H^+_{\gamma K}(k\rho)\right], \tag{10}$$

where $H^{\pm}_{\gamma K}(x)$ are Hankel functions [28] and $U^{J\pi}_{\gamma K,\gamma' K'}$ is the three-body collision matrix. We use the R-matrix method to calculate those states with appropriate boundary conditions [19].

C. The *R*-matrix method

The R-matrix theory provides an efficient way of solving the Schrödinger equation at positive energies. Here, we briefly discuss the R-matrix formalism to find three-body scattering states with the correct asymptotic conditions [18,19]. An extensive review is presented in Ref. [22].

The basic idea of the R-matrix method is to divide the configuration space into two regions: an internal region with ρ within the interval $[0, a]$, where nuclear, Coulomb, and centrifugal interactions act, and an external region, from the channel radius a, where the nuclear interaction is negligible. The internal wave function is expanded on a variational basis as in Eq. (8), and it is matched at $\rho = a$ with the external wave function (10).

For three-body systems, it is known that the nuclear interaction is not negligible until large ρ values [see Eq. (7)], which are typically of several hundreds of fm (see Ref. [19]). Therefore, the internal region is split into two regions. In the interval $[0, a_0]$ the numerical values of the potential are used, and the wave functions are expanded over basis (8). In the intermediate region $[a_0, a]$, approximations of the potentials make it easier to use propagation methods [22]. In this way there is no need for large variational bases. The collision matrix is calculated from the R-matrix evaluated at the channel radius a.

For three-body scattering, because the particles can share the angular momentum in an infinite number of ways, the dimension of the scattering matrix is infinite. In practical calculations, the dimension depends on $K_{\max}$. For large values, the typical dimension of the collision matrix is of the order of $\sim$100$-$200.

D. Pseudostates

The R-matrix method provides an efficient way to deal with two-body continuum states with the correct boundary conditions. However, R-matrix calculations for three-body systems in hyperspherical coordinates are tedious because of the long range (7) of the nuclear potentials. An alternative method that avoids the introduction of the three-body scattering conditions is the pseudostate method [29]. It is an approximate method where the continuum is discretized, and it is based on the extension of variational calculations to positive energies.

In the present case, we expand the hyper-radial wave function (8) on a square integrable basis, and we introduce this expansion into the coupled differential equations (6) to end up with an eigenvalue problem from which we get the coefficients $c^{J\pi}_{\gamma Ki}$ for each eigenvalue. Therefore, from the diagonalization of H_{3b} we find the ground state $\Psi^{J_0M_0\pi_0}$ at $E_0 < 0$ and a set of pseudostates $\Psi^{J\pi}_{\lambda}(E^{J\pi}_{\lambda})$ defined at positive energies.

E. Forbidden states

Forbidden states appear in microscopic cluster models from the full antisymmetrization of the wave function. Those states are typically simulated in nonmicroscopic models by additional bound states in the effective core + nucleon interaction. These unphysical forbidden states introduce spurious eigenvalues in the spectrum of the three-body Hamiltonian, and therefore they have to be removed.

In the literature, essentially two methods are available to remove forbidden states [18]: the projection technique [30] and the supersymmetric transform [31] of the core + n interaction. The former consists of adding a projector operator to the two-body potential to project out the forbidden states and then solving the Schrödinger equation in the allowed space. In the supersymmetric transform, the deep core + n interaction is replaced by a shallow potential with the same scattering properties, but without the forbidden states.

The projection technique is difficult to apply to three-body scattering states. The nonlocality of the projector makes difficult the implementation of propagation techniques in the R-matrix formalism described above. Therefore, to find three-body bound and scattering states we use a supersymmetry transform of the core + n potential.

F. *E*1 strength

The $E1$ strength distribution for transitions from the ground state with energy $E_0 < 0$, total angular momentum J_0, projection M_0, and parity π_0, through the electric dipole $\mathcal{M}^{(E1)}_{\mu}$ operator, to a continuum final state, is defined as

$$\frac{dB(E1)}{dE} = \frac{1}{2J_0+1} \times \sum_{S\nu M_0\mu} \int d\boldsymbol{k}_x d\boldsymbol{k}_y\, \delta\left[E - \frac{\hbar^2}{2m_N}\left(k_x^2 + k_y^2\right)\right] \times |\langle \Psi^{(-)}_{\boldsymbol{k}_x,\boldsymbol{k}_y,S\nu}(E,\boldsymbol{x},\boldsymbol{y})|\mathcal{M}^{(E1)}_{\mu}|\Psi^{J_0M_0\pi_0}(\boldsymbol{x},\boldsymbol{y})\rangle|^2, \tag{11}$$

where the dipole operator reads

$$\mathcal{M}^{(E1)}_{\mu} = eZ_1\left(\frac{2}{A_1(A_1+2)}\right)^{1/2} y Y^{\mu}_1(\Omega_y). \tag{12}$$

Here $\Psi^{(-)}_{\boldsymbol{k}_x,\boldsymbol{k}_y,S\nu}$ is a three-body scattering state with ingoing boundary conditions. This state is related to the scattering state defined in Eq. (9) through a time-reversal operation [17].

In the discretized-continuum approximation, the $B(E1)$ strength distribution becomes

$$\frac{dB(E1)}{dE} \approx \sum_{J\pi\lambda} f\left(E, E^{J\pi}_{\lambda}\right) B_{E1}\left(J_0\pi_0 \to J\pi, E^{J\pi}_{\lambda}\right), \tag{13}$$

where

$$B_{E1} = \frac{2J+1}{2J_0+1}\left|\langle \Psi^{J\pi}_{\lambda}\left(E^{J\pi}_{\lambda}\right)||\mathcal{M}^{E1}||\Psi^{J_0\pi_0}\rangle\right|^2 \tag{14}$$

is the reduced $E1$ transition probability from the ground state $\Psi^{J_0\pi_0}$ to a pseudostate $\Psi^{J\pi}_{\lambda}(E^{J\pi}_{\lambda})$. The function $f(E, E^{J\pi}_{\lambda})$ is a smearing function introduced to smooth the discrete B_{E1} values. This function is, in general, a Gaussian or a Lorentzian (see Ref. [23] for more detail).

III. REACTIONS IN THE FOUR-BODY EIKONAL METHOD

A. Wave functions

We closely follow the formalism described in Ref. [17] to study the elastic breakup and the elastic scattering of a Borromean nucleus in a four-body eikonal model. Let us consider the four-body Schrödinger equation

$$H_{4b}\Phi(\boldsymbol{R},\boldsymbol{x},\boldsymbol{y}) = E_T\Phi(\boldsymbol{R},\boldsymbol{x},\boldsymbol{y}), \tag{15}$$

with

$$H_{4b} = -\frac{\hbar^2}{2\mu_{PT}}\Delta_R + H_{3b} + V_{PT}(\boldsymbol{R},\boldsymbol{x},\boldsymbol{y}). \tag{16}$$

Here H_{3b} is the internal Hamiltonian (3) of the three-body projectile, $\boldsymbol{R} = (\boldsymbol{b}, Z)$ is the relative coordinate between the center of mass of the projectile and the center of mass of the target, and μ_{PT} is the projectile-target reduced mass. The total energy of the four-body system is defined from the ground-state energy of the projectile E_0 as

$$E_T = \frac{\hbar^2}{2\mu_{PT}}K^2 + E_0, \tag{17}$$

where $\boldsymbol{K}$ is the initial wave vector of the projectile-target relative motion along Z. The projectile-target interaction that considers nuclear, as well Coulomb interactions, is taken as $V_{PT} = \sum_{i=1}^{3} V_{iT}(\boldsymbol{R},\boldsymbol{x},\boldsymbol{y})$, where $i = 1$ labels the core, and $i = 2, 3$ the external neutrons. Those interactions are simulated with complex optical potentials.

The standard procedure in the eikonal approximation is to factorize the wave function as

$$\Phi(\boldsymbol{R},\boldsymbol{x},\boldsymbol{y}) = e^{iKZ}\hat{\Phi}(\boldsymbol{R},\boldsymbol{x},\boldsymbol{y}). \tag{18}$$

This factorization is introduced in Eq. (15) with the adiabatic approximation that consists of replacing H_{3b} by E_0 [5]. The eikonal wave function, valid at high energies, is given by

$$\hat{\Phi}_{\text{eik.}}(\boldsymbol{R},\boldsymbol{x},\boldsymbol{y}) = \exp\left[-\frac{i}{\hbar v}\int_{-\infty}^{Z} dZ'\, V_{PT}(\boldsymbol{b},Z',\boldsymbol{x},\boldsymbol{y})\right] \times \Psi^{J_0M_0\pi_0}(\boldsymbol{x},\boldsymbol{y}), \tag{19}$$

where v is the relative velocity between the target and the projectile.

B. Elastic and breakup cross sections

The breakup cross section is related to transition matrix elements. In eikonal calculations, one introduces the wave function given by Eqs. (18) and (19) in the transition matrix element, and one assumes that the transferred wave vector $\boldsymbol{q} = \boldsymbol{K}' - \boldsymbol{K}$ is orthogonal to the initial wave vector $\boldsymbol{K}$. This procedure leads to

$$T_{fi} = i\hbar v\int d^2\boldsymbol{b}\, e^{-i\boldsymbol{q}\cdot\boldsymbol{b}} S_{Sv}(E,\boldsymbol{k}_x,\boldsymbol{k}_y,\boldsymbol{b}), \tag{20}$$

with the eikonal breakup amplitudes described by

$$S_{Sv} = \left(\frac{A_1+2}{A_1}\right)^{3/4}\langle\Psi^{(-)}_{\boldsymbol{k}_x,\boldsymbol{k}_y,Sv}|e^{i\chi(\boldsymbol{b},\boldsymbol{b}_x,\boldsymbol{b}_y)}|\Psi^{J_0M_0\pi_0}\rangle, \tag{21}$$

and depends on the initial three-body bound state $\Psi^{J_0M_0\pi_0}$ and on the final three-body scattering state $\Psi^{(-)}_{\boldsymbol{k}_x,\boldsymbol{k}_y,Sv}$. The dynamics information is contained in the eikonal phase

$$\chi(\boldsymbol{b},\boldsymbol{b}_x,\boldsymbol{b}_y) = -\frac{1}{\hbar v}\int_{-\infty}^{\infty} dZ\sum_{i=1}^{3} V_{iT}(\boldsymbol{b},Z,\boldsymbol{b}_x,\boldsymbol{b}_y), \tag{22}$$

where $\boldsymbol{b}_x$ and $\boldsymbol{b}_y$ are the transverse components of $\boldsymbol{x}$ and $\boldsymbol{y}$, respectively. For $i = 1$, V_{1T} does not depend on $\boldsymbol{b}_x$.

From the above definition we see that the eikonal phase can be separated into its nuclear and Coulomb contributions. Therefore, we rewrite this equation as

$$\chi = \chi^N + \chi^C_{PT} + \chi^C. \tag{23}$$

Here χ^N is the nuclear eikonal phase, and χ^C_{PT} is the Coulomb eikonal phase between the target and the projectile. The tidal Coulomb eikonal phase χ^C is attributable to the distortion of the projectile and reads

$$\chi^C = -\frac{1}{\hbar v}\int_{-\infty}^{\infty} dZ\left(V^C_{1T} - \frac{Z_TZ_Pe^2}{R}\right), \tag{24}$$

where V^C_{1T} stands for the core-target Coulomb interaction, and where Z_Pe and Z_Te are the charges of the projectile and target, respectively.

The Coulomb eikonal phase leads to two divergence problems. The first divergence comes from the integral defining χ^C_{PT}. It has been fixed by introducing a cutoff [4,5] and this phase is given by

$$\chi^C_{PT} = 2\eta\ln(Kb), \tag{25}$$

plus an additional term which becomes just a phase factor playing no role in the cross sections (η is the Sommerfeld parameter). The second divergence is related to the term χ^C because it behaves as $1/b$ at large distances, and therefore the breakup cross section diverges logarithmically [5].

The adiabatic approximation is responsible of the divergence associated with the term χ^C. In fact, it is the first order of the expansion in $e^{i\chi^C}$ which leads to the aforementioned divergence. Hence, a valid method to avoid it is to replace the first-order term of this expansion by the first order of the perturbation theory [7,8]. This provides

$$e^{i\chi} \to e^{i\chi^N}(e^{i\chi^C} - i\chi^C + i\chi^{FO})e^{i\chi^C_{PT}}. \tag{26}$$

As the adiabatic approximation is not performed in perturbation theory, the term χ^{FO} does not diverge. This method is referred to as a Coulomb-corrected eikonal approximation and has been applied to describe breakup reactions involving halo nuclei in Refs. [9,17].

In practice, the eikonal phase factor $e^{i\chi}$ of Eq. (21) is expanded in multipole components to calculate transition matrix elements, from which differential cross sections are derived (see Ref. [17]).

Elastic scattering cross sections in a four-body eikonal model are deduced in a similar way. The elastic scattering amplitude is given by

$$f_{M_0',M_0} = \frac{iK}{2\pi}\int d^2\boldsymbol{b}e^{-i\boldsymbol{q}\cdot\boldsymbol{b}}\left[\delta_{M_0'M_0} - S^{J_0}_{M_0'M_0}(\boldsymbol{b})\right], \tag{27}$$

where

$$S^{J_0}_{M'_0 M_0}(\boldsymbol{b}) = \langle \Psi^{J_0 M'_0 \pi_0} | e^{i\chi(\boldsymbol{b},\boldsymbol{b}_x,\boldsymbol{b}_y)} | \Psi^{J_0 M_0 \pi_0} \rangle. \quad (28)$$

As before, the factor $e^{i\chi}$ is expanded in multipoles and as usual, a rearrangement of the Coulomb terms has been done for the numerical calculations (see Ref. [17] for detail).

IV. CONDITIONS OF THE CALCULATIONS

A. ^{11}Li structure

We assume a three-body model with a spinless ^{9}Li core. To calculate bound and continuum states, we need core + n and $n + n$ interactions. As $^9\text{Li} + n$ potential we choose that of Ref. [32], which contains central and spin-orbit terms with a Woods-Saxon shape. This interaction generates a core + n s-wave scattering length of -5.7 fm. It also reproduces a $p_{1/2}$ resonance near 540 keV, in agreement with Ref. [33]. This interaction contains two forbidden states ($s_{1/2}$ and $p_{3/2}$) which are eliminated through supersymmetric transformations. The $n + n$ potential is the central part of the Minnesota interaction with the standard value $u = 1$ [34]. It reproduces the binding energy of the deuteron and the $n + n$ scattering length.

The $^9\text{Li} + n$ and $n + n$ interactions give a ^{11}Li ground-state energy of $E_0 = -0.29$ MeV. To reproduce the most recent experimental value of -0.378 MeV [10], we slightly modified the core + n optical potential by multiplying it by a factor $\lambda_{cn} = 1.0051$. This factor is very close to unity and does not affect the properties of the $^9\text{Li} + n$ system (the scattering length is -6.3 fm). The same potential has been used for all partial waves. Using a core radius of 2.43 fm [35], the rms radius of ^{11}Li is 3.2 fm, in agreement with the experimental value of 3.16 ± 0.11 fm [36].

We follow Ref. [19] to calculate continuum states and eigenphases. Adopting the same notations, the common parameters that involve ground-state and continuum wave functions are those defining the Lagrange-Legendre functions: the channel radius a_0 and the number of Lagrange functions N. In all cases, the propagation technique is implemented up to a channel radius $a = 400$ fm. We performed various tests to check the stability of the results (phase shifts and $E1$ strengths) when these parameters vary. The sum over K in the 0^+ ground state is truncated at $K_{\max} = 40$. For continuum scattering states, we consider the most dominant partial waves $J = 0^+, 1^-, 2^+$ with corresponding $K_{\max} = 32, 25, 22$, respectively. The corresponding numbers of channels [i.e., the numbers of coupled equations in system (6)] are 153, 260, and 319 for $J = 0^+, 1^-$, and 2^+, respectively.

B. Reaction framework

To study the elastic scattering and breakup of ^{11}Li on ^{208}Pb at 70 MeV/nucleon, we need $^9\text{Li} + {}^{208}\text{Pb}$ and $n + {}^{208}\text{Pb}$ nuclear optical potentials at the corresponding energies. For the $n + {}^{208}\text{Pb}$ interaction, we consider the central part of the complex optical potential given in Ref. [37] at 70 MeV.

The choice of the core-target interaction is more complicated because of the lack of elastic-scattering data in the literature. To estimate this potential, we proceed as in Ref. [38]. In this reference, the ^{10}Be-^{208}Pb potential needed to study the breakup of ^{11}Be was taken as the α-^{208}Pb optical potential with a scaled radius. We follow here the same procedure, and use the α-^{208}Pb of Bonin *et al.* [39] at 699 MeV. For the $^9\text{Li} + {}^{208}\text{Pb}$ potential, the scaled radii for the real and imaginary components are $R_r = 7.36$ fm and $R_i = 7.12$ fm, respectively. The conditions to calculate elastic, breakup and double differential cross sections are identical to those described in Ref. [17] for ^{6}He.

V. RESULTS AND DISCUSSION

A. $^9\text{Li} + n + n$ eigenphases

Figure 1 displays the dominant 0^+, 1^-, and 2^+ eigenphases [19] of $^9\text{Li} + n + n$. The 0^+ and 2^+ curves exhibit a wide rise in energy with a resonantlike behavior. Particularly, the 0^+ phase shifts show two bumps around 0.2 and 1.0 MeV that may indicate overlapping resonances. A low-lying 0^+ resonance has also been predicted in Refs. [12,13]. The 1^- eigenphase shows a sharp resonant behavior around 0.5 MeV. This energy is consistent with the maximum observed in the breakup experimental data (see below) and suggests the existence of a low-lying resonance in ^{11}Li.

B. $E1$ strength distributions

In Fig. 2, we test the convergence of the $E1$ strength distributions (11), and show the results for different $K_{\max}$ values. We can observe enhanced $E1$ strength distributions with a peak position near 0.5 MeV for $K_{\max} = 25$. This peak is consistent with the 1^- eigenphase and supports the existence of a 1^- resonance close to threshold. The comparison between $K_{\max} = 23$ and $K_{\max} = 25$ shows that the convergence is fairly good. Low $K_{\max}$ values are illustrated with $K_{\max} = 13$. Under those conditions, the resonance energy is shifted to 0.65 MeV.

Figure 3 displays convoluted $E1$ strength distributions. We also show the $E1$ strength distributions calculated with the pseudostate method [Eq. (13)]. It is widely employed in the literature (see, for example, Ref. [20]). As in Ref. [23],

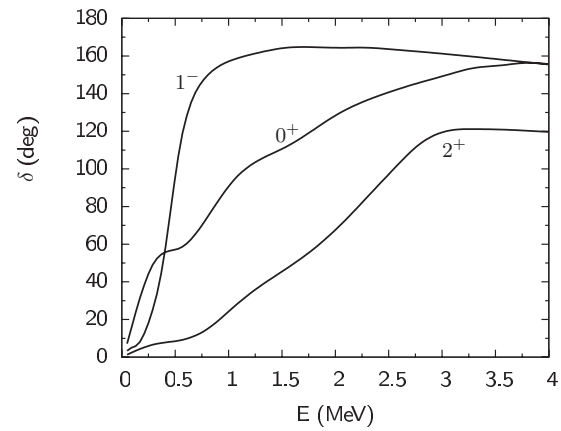

FIG. 1. Dominant 0^+, 1^-, and 2^+ eigenphases of the $^9\text{Li} + n + n$ system.

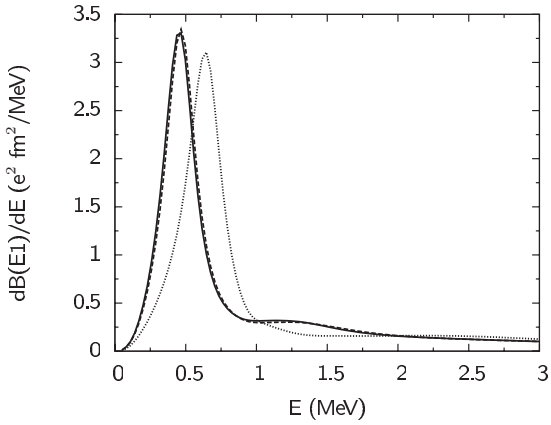

FIG. 2. $E1$ strength distribution calculated with the R-matrix method for $K_{max} = 25$ (solid line), $K_{max} = 23$ (dashed line), and $K_{max} = 13$ (dotted line).

we use a Lagrange-Laguerre basis with $N = 70$ and a scaling factor $h = 0.3$ fm. Various tests have been performed to check the stability of the results with respect to these parameters. To be consistent with R-matrix results, we eliminate the forbidden states through supersymmetric transforms of the core + n potential.

The convolution of the theoretical $E1$ strength and breakup cross sections are done by considering a Gaussian response function [2]. Three typical σ values are chosen: $\sigma = 0.05$ MeV, which is close to zero but allows the use of the PS method; $\sigma = 0.17\sqrt{E}$ MeV (normalized in energy between 0 and ∞), which corresponds to the energy resolution quoted in Ref. [2]; and $\sigma = 0.31$ MeV, which provides the optimal fit to the data.

With the experimental resolution $\sigma = 0.17\sqrt{E}$ MeV, we overestimate the $E1$ strength derived by Nakamura *et al.* [2] from their experimental breakup cross sections below 1 MeV, and the peak position of our prediction is slightly shifted with respect of the experimental data. Our results are similar to those obtained by Esbensen *et al.* [24], who use different interactions. We do not predict a possible bump near 1.2 MeV, as suggested by experiment. Beyond 1.5 MeV, the present

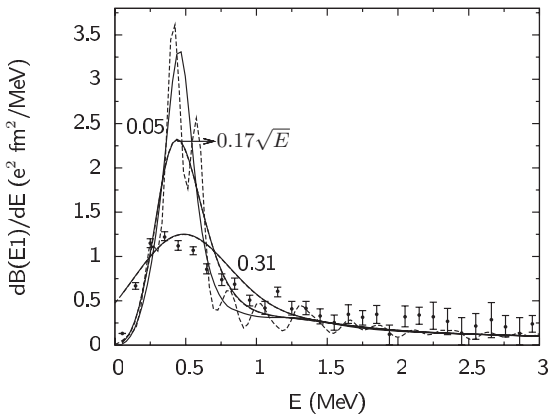

FIG. 3. $E1$ strength distribution calculated with the R-matrix (solid lines) and pseudostate (dashed lines) methods. The calculations are convoluted with a Gaussian function and with three different σ values (labels, in MeV). Experimental data are taken from Ref. [2].

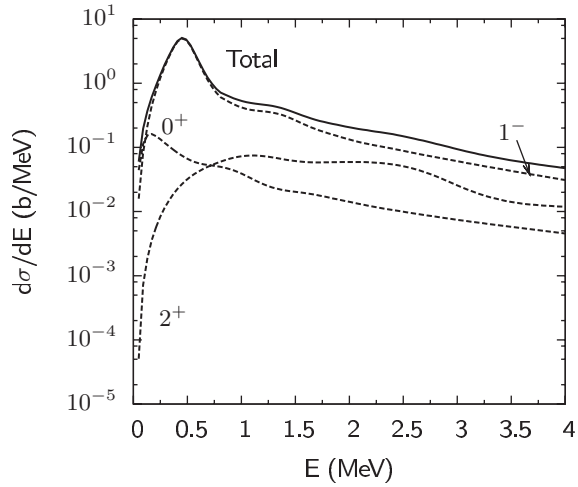

FIG. 4. Total breakup cross section (solid line) of ^{11}Li on ^{208}Pb at 70 MeV/nucleon and its partial-wave decomposition (dashed lines).

model does reproduce the experimental energy dependence, but slightly underestimates the data. This problem might be attributable to inelastic-breakup events, which are not included in the calculation.

The R-matrix and pseudostate approaches are in very good agreement with each other, except for the artificial oscillations in the pseudostate method, caused by a folding with small σ values. In the peak region, the difference between both methods is less than 1% and the amplitude varies with σ. The value $\sigma = 0.31$ MeV gives a good fit of the experimental data but introduces a nonzero dipole strength at $E = 0$ MeV. However, the choice of this value is somewhat artificial and is not directly related to the detector resolution.

The good agreement between both methods indicates that the difference between the theoretical convoluted curve of Fig. 3 and the experimental data does not come from the R-matrix calculation. In contrast with breakup cross sections, $E1$ strengths are not directly measurable. Therefore, their determination is partly model dependent. We come back in Sec. VI to the model assumptions used for the experimental determination of the $B(E1)$ distribution.

C. Breakup cross sections and angular distributions

In this section, we study the elastic breakup of ^{11}Li on ^{208}Pb at 70 MeV/nucleon with a four-body eikonal model. The total eikonal cross section $d\sigma/dE$ and its partial wave decomposition are shown in Fig. 4. They are calculated with Eqs. (51) and (52) of Ref. [17]. As expected for a breakup dominated by the Coulomb field, the total cross section is mainly of 1^- character. It presents a peak around 0.5 MeV, which is also seen in the 1^- partial cross section. It corresponds to the resonance in the 1^- eigenphase and to the narrow peak of the dipole strength distribution. Beyond this peak, the 0^+ and 2^+ contributions are not negligible. In particular, the 2^+ component represents more than 10% of the total cross section at 4 MeV.

The behavior of the partial cross sections is better illustrated in Fig. 5. For the 0^+ partial wave, we can see a narrow peak

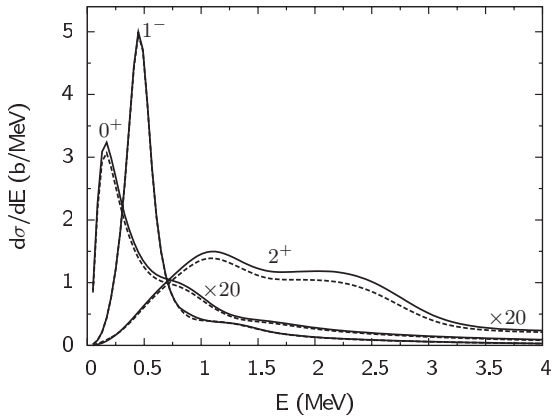

FIG. 5. Breakup cross sections of the 0^+, 1^-, 2^+ partial waves. The dashed curves correspond to a modified ^{9}Li-target potential as described in Sec. V D.

around 0.25 MeV and a second wider structure around 1 MeV. Those peaks coincide with the positions of the bumps observed in the eigenphases of Fig. 1. A similar prediction for the 0^+ excitation energy spectrum was suggested by Ershov *et al.* [40] from the study of the excitation energy spectrum of ^{11}Li colliding on a proton target at 68 MeV/nucleon. The 2^+ partial cross section exhibits two broad peaks, near 1.2 and 2.5 MeV, in agreement with the 2^+ eigenphases of Fig. 1.

Figure 6 displays the total and 1^- breakup cross sections of Fig. 4 convoluted with the detector response and compared with the experimental data of Ref. [2]. We observe a fair agreement for energies above 1.5 MeV, but the peak energy is slightly too high in the model. The conditions of the calculation have been determined on the 0^+ ground state, and no fitting procedure is applied to the 1^- partial wave. Including the 0^+ and 2^+ contributions increases the total cross section beyond 1 MeV, in better agreement with the experimental data. In the literature, calculations of breakup cross sections of halo nuclei often use the equivalent photon method [41]. This approximation assumes a dipole breakup process and ignores

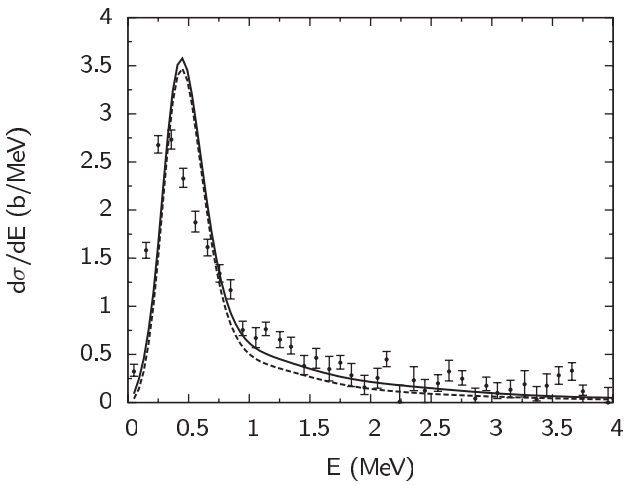

FIG. 6. Total breakup cross section (solid line) and 1^- contribution (dashed line) convoluted with the detector response. Experimental data are taken from Ref. [2].

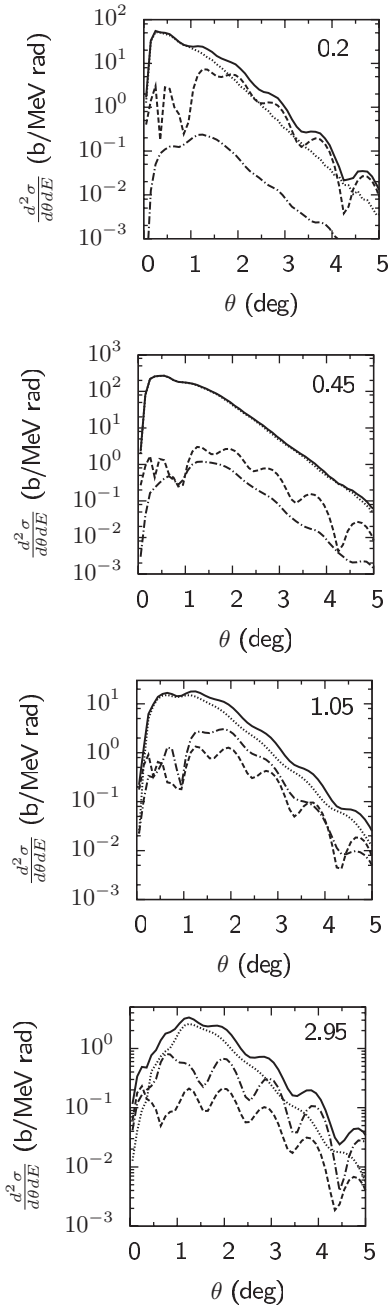

FIG. 7. Double differential cross sections (solid lines) as a function of the scattering angle with their partial-wave decomposition at different excitation energies (top labels in MeV). The dashed, dotted, and dash-dotted lines correspond to the 0^+, 1^-, and 2^+ partial waves, respectively.

other contributions. In contrast, the present eikonal description of the breakup reaction is more accurate, because it allows a quantitative evaluation of other partial wave contributions.

A further investigation of the excitation multipoles and mechanism is shown in the double differential cross sections, $\frac{d^2\sigma}{d\theta dE}$ (Eq. (50) of Ref. [17]), as a function of the scattering angle, and at different excitation energies. In Fig. 7, we display the cross section and its partial-wave decomposition for four excitation energies: 0.2 MeV, near the 0^+ narrow peak;

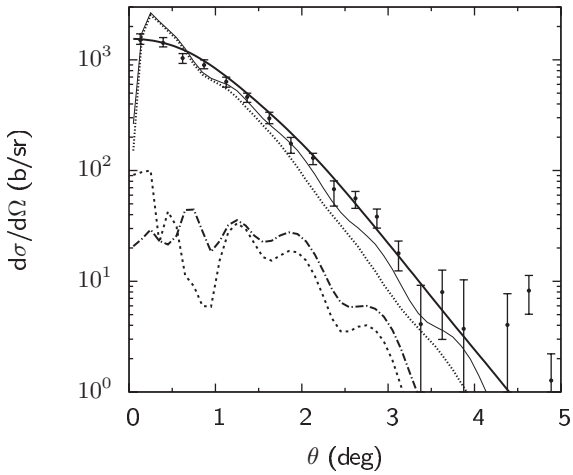

FIG. 8. Total angular distribution (thin solid line) for the breakup of ^{11}Li on ^{208}Pb at 70 MeV/nucleon in the range $0 \leqslant E \leqslant 4$ MeV, and its decomposition in the dominant partial waves 0^+ (dashed), 1^- (dotted), and 2^+ (dash-dotted). The thick solid line shows the total angular distribution convoluted with the detector resolution. The experimental data are taken from Ref. [2].

0.45 MeV, close to the 1^- narrow peak; 1.05 MeV, around the 0^+ wide peak; and 2.95 MeV, presumably far from resonances.

At all energies the 0^+ partial cross section presents diffraction patterns at large angles ($\theta \gtrsim 1^\circ$). At 0.2 MeV, for very forward angles ($\theta \lesssim 1^\circ$), the total double differential cross section is practically of 1^- character, but at larger angles, there is a strong influence of the 0^+ partial contribution supporting the indication of a 0^+ resonance. As expected, at 0.45 MeV, the dipole contribution is strongly dominant. Conversely, at $E = 1.05$ MeV, the 0^+ and 2^+ contributions are not negligible at large angles. Around 3 MeV the 2^+ and 1^- components have the same order of magnitude at large angles.

Energy-integrated cross sections are available experimentally. They are defined as

$$\frac{d\sigma}{d\Omega} = \int_0^{E_{\max}} \frac{d^2\sigma}{d\Omega dE} dE. \tag{29}$$

In Fig. 8 we show this total angular distribution for $E_{\max} = 4$ MeV, which corresponds to the experimental conditions [2]. The theoretical cross section is convoluted by a Gaussian function (with a width of 0.44°) to simulate the experimental angular resolution. For all scattering angles the 1^- partial wave dominates, and the total angular distribution is mainly 1^- at very small angles. The agreement between the experimental data and the convoluted theoretical curve is quite good for almost all angles, even though there is no free parameter in our calculations.

Figure 9 presents double differential cross sections with respect to two-body energies (see Ref. [17] for detail). In the top panel, E_{21} and $E_{c(21)}$ are the energies between the external neutrons and between their c.m. and the core. These energies correspond to the "dineutron" or "T" configuration. The "Y" configuration is characterized by E_{1c}, the relative energy between a neutron and the ^{9}Li core, and by $E_{2(c1)}$, the energy between neutron 2 and the c.m. of the ^{10}Li $=^9$ Li $+ n$ system.

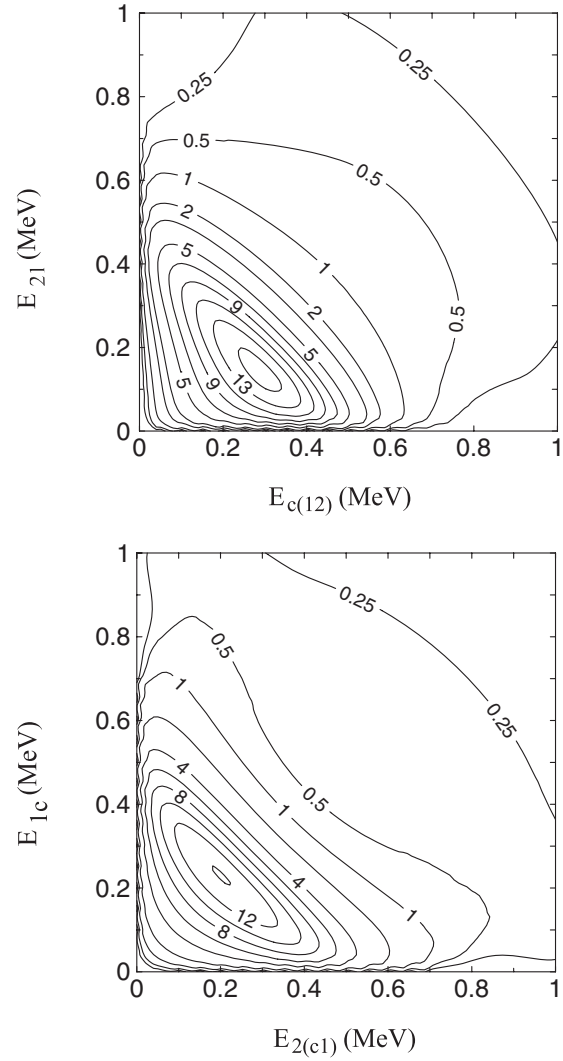

FIG. 9. (Top) 1^- component of the double-differential cross sections $d^2\sigma/dE_{21}dE_{c(12)}$ in b/MeV^2 as a function of partial energies E_{21} and $E_{c(12)}$ for ^{11}Li breakup on ^{208}Pb at 70 MeV/nucleon. (Bottom) Same as top panel for $d^2\sigma/dE_{1c}dE_{2(c1)}$.

These cross sections provide information about correlations in ^{11}Li.

In the T configuration (top panel of Fig. 9), a maximum is obtained near $E_{21} = 0.15$ MeV and $E_{c(21)} = 0.3$ MeV. This peak might correspond to the neutron-neutron virtual state. In the Y configuration (bottom panel of Fig. 9), there is a maximum near $E_{1c} \approx E_{2(c1)} \approx 0.2$ MeV. Experimental measurements would be helpful to clarify the structure of the 1^- resonance.

D. Influence of the nucleus-target potentials

The ^{9}Li-^{208}Pb potential is poorly known and has been determined here from a scaling of an optical α-^{208}Pb potential. To test the sensitivity of the breakup cross section to this potential, we multiply it by a factor of two. The dependence is illustrated by the dashed curves of Fig. 5. For all partial waves,

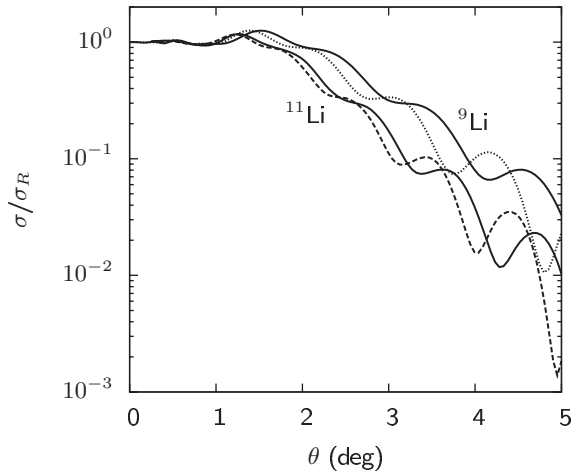

FIG. 10. Elastic scattering angular distributions of ^{11}Li and ^{9}Li on ^{208}Pb in the present four-body eikonal model and in a two-body eikonal model at 70 MeV/nucleon, respectively. The solid lines correspond to the original ^{9}Li-target potential, and the dashed and dotted lines are obtained with the modified ^{9}Li-target potential (see text).

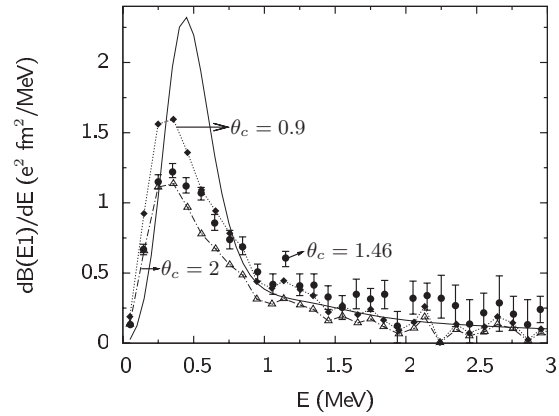

FIG. 11. Dependence of the experimental $B(E1)$ strength distribution on θ_c (in degrees). The circles correspond to the conditions of Ref. [2], and the triangles and squares correspond to other choices of θ_c (the lines are to guide the eye). The solid line corresponds to the present model with the experimental energy resolution.

we do not get an appreciable dependence on the breakup cross section by the choice of the core-target potential.

The same sensitivity is studied in Fig. 10 for elastic scattering. We present the calculations for the ^{9}Li-^{208}Pb and ^{11}Li-^{208}Pb collisions. In contrast with the breakup cross section, the elastic scattering is more dependent on the core-target potential. For a given potential, we find a reduction of the elastic scattering of ^{11}Li in comparison with the elastic scattering of ^{9}Li. This behavior may indicate a reduction of the ^{11}Li elastic scattering owing to flux going to the breakup channel.

VI. DERIVATION OF THE $E1$ STRENGTH DISTRIBUTION

The experimental $E1$ strength distribution of ^{11}Li is extracted from the breakup cross section by using the equivalent photon method [41], which assumes a Coulomb-dominated $E1$ breakup process. With this assumption, let us study the sensitivity of the experimental data to the way the nuclear contribution is excluded.

In a nonrelativistic regime, the electric dipole strength is related with the breakup cross section by Ref. [5]

$$\frac{dB(E1)}{dE} = \frac{9}{32\pi}\left(\frac{\hbar v}{Z_T e}\right)^2 \frac{1}{\xi K_0(\xi) K_1(\xi)} \frac{d\sigma}{dE}, \tag{30}$$

with the adiabaticity parameter

$$\xi = \frac{E - E_0}{\hbar v} b_{\min}. \tag{31}$$

The minimal impact parameter is

$$b_{\min} = \frac{Z_P Z_T e^2}{2E_{PT}\tan(\theta_c/2)}, \tag{32}$$

where E_{PT} is the projectile-target relative energy, and θ_c stands for the maximal cutoff scattering angle up to which the breakup process is Coulomb dominated. It is chosen from the experimental breakup angular distribution [2]. According to Figs. 8 and 10, the present model suggests a Coulomb dominated angular range for $\theta \lesssim 0.9^\circ$. We therefore adopt $\theta_c = 0.9^\circ$.

To estimate the dependence of the $B(E1)$ strength distribution on θ_c, we recalculate the dipole strength using Eq. (30) and the experimental breakup data of Ref. [2]. We choose the values $\theta_c = 2^\circ$ and $\theta_c = 0.9^\circ$, above and below the value $\theta_c = 1.46^\circ$ reported in Ref. [2]. Those values correspond to $b_{\min}$ values of 14 and 31 fm, respectively. The results are displayed in Fig. 11, from which we can observe an enhancement of the $E1$ strength distribution at low excitation energies for $\theta_c = 0.9^\circ$. This result is closer to our calculation (solid line in Fig. 11), and the difference between theory and experiment is now similar to the difference obtained in the breakup cross sections (Fig. 4).

We therefore suggest that the experimental $E1$ strength is underestimated. To get reliable dipole strengths, it is necessary for the extraction of the $B(E1)$ strength distribution to consider more elaborate reaction models including nuclear and Coulomb effects as well as their interference consistently.

VII. CONCLUSION

We have investigated the ^{11}Li breakup in the eikonal approximation, with a $^{9}\mathrm{Li} + n + n$ three-body description of the projectile. We use the hyperspherical formalism and expand the hyper-radial functions on a Lagrange basis. Combined with the R-matrix theory, the model provides a simultaneous description of three-body bound and scattering states. This is crucial for breakup calculations which involve both types of wave functions.

The $^{9}\mathrm{Li} + n + n$ phase shifts suggest the existence of a narrow 1^- resonance near $E = 0.5$ MeV, corresponding to $E_x \approx 0.9$ MeV. Taking into account the $3/2^-$ spin of the ^{9}Li core nucleus, this resonance should correspond to $J = 1/2^+$, $3/2^+$, or $5/2^+$ in ^{11}Li. The existence of such a resonance

is supported by a low-energy maximum in the experimental breakup cross section. At low energies, our resonance energy is slightly higher than that seen experimentally, but there is a qualitative agreement with the data. Beyond 1 MeV, we underestimate the data, which contain inelastic breakup events. The importance of this inelastic contribution is difficult to evaluate, but is partly responsible for the difference between theory and experiment. In this energy range we have shown that the monopole and quadrupole components are not negligible and may represent up to ≈15% of the total cross section.

Surprisingly the agreement between theory and experiment for the $E1$ strength distribution is less good in the resonance region. We have addressed this apparent inconsistency by redetermining the $E1$ strength from the experimental breakup cross sections and by going beyond the simple dipole Coulomb approximation. We have suggested that the $E1$ experimental data of Nakamura *et al*. [2] are affected by this approximation. Detailed comparisons between experiment and theory should therefore be done on the breakup cross sections, rather than on the $E1$ distributions.

The existence of a dipole resonance in the ^{11}Li nucleus seems now to be well established from experiment as well as from theory. The situation is less clear in ^{6}He [17], where a 1^- resonance (broader than in ^{11}Li) is predicted by most theories, but not yet observed by experiment [42]. Let us finally mention that elastic-scattering experiments at the same energy would be very useful to assess the precision of the model and, indirectly, of the predicted breakup cross sections.

ACKNOWLEDGMENTS

This text presents research results of the IAP program P6/23 initiated by the Belgian-state Federal Services for Scientific, Technical, and Cultural Affairs. E.C.P. is supported by the IAP program. P.D. acknowledges the support of F.R.S.-FNRS, Belgium.

[1] P. G. Hansen, A. S. Jensen, and B. Jonson, Annu. Rev. Nucl. Sci. **45**, 591 (1995).
[2] T. Nakamura *et al*., Phys. Rev. Lett. **96**, 252502 (2006).
[3] M. Yahiro, Y. Iseri, H. Kameyama, M. Kamimura, and M. Kawai, Prog. Theor. Phys. Suppl. **89**, 32 (1986).
[4] R. J. Glauber, *in Lectures in Theoretical Physics*, edited by W. E. Brittin and L. G. Dunham, Vol. 1 (Interscience, New York, 1959), p. 315.
[5] Y. Suzuki, R. G. Lovas, K. Yabana, and K. Varga, *Structure and Reactions of Light Exotic Nuclei* (Taylor & Francis, London, 2003).
[6] M. Yahiro, K. Ogata, and K. Minomo, Prog. Theor. Phys. **126**, 167 (2011).
[7] J. Margueron, A. Bonaccorso, and D. M. Brink, Nucl. Phys. A **720**, 337 (2003).
[8] B. Abu-Ibrahim and Y. Suzuki, Prog. Theor. Phys. **112**, 1013 (2004).
[9] P. Capel, D. Baye, and Y. Suzuki, Phys. Rev. C **78**, 054602 (2008).
[10] C. Bachelet, G. Audi, C. Gaulard, C. Guénaut, F. Herfurth, D. Lunney, M. de Saint Simon, and C. Thibault, Phys. Rev. Lett. **100**, 182501 (2008).
[11] I. Tanihata, J. Phys. G **22**, 157 (1996).
[12] I. J. Thompson, B. V. Danilin, V. D. Efros, M. V. Zhukov, and J. S. Vaagen, J. Phys. G **24**, 1505 (1998).
[13] R. Crespo, I. J. Thompson, and A. A. Korsheninnikov, Phys. Rev. C **66**, 021002 (2002).
[14] T. Myo, S. Aoyama, K. Katō, and K. Ikeda, Phys. Lett. B **576**, 281 (2003).
[15] M. V. Zhukov, B. V. Danilin, D. V. Fedorov, J. M. Bang, I. J. Thompson, and J. S. Vaagen, Phys. Rep. **231**, 151 (1993).
[16] P. Descouvemont, C. Daniel, and D. Baye, Phys. Rev. C **67**, 044309 (2003).
[17] D. Baye, P. Capel, P. Descouvemont, and Y. Suzuki, Phys. Rev. C **79**, 024607 (2009).
[18] I. J. Thompson, B. V. Danilin, V. D. Efros, J. S. Vaagen, J. M. Bang, and M. V. Zhukov, Phys. Rev. C **61**, 024318 (2000).
[19] P. Descouvemont, E. M. Tursunov, and D. Baye, Nucl. Phys. A **765**, 370 (2006).
[20] K. Hagino and H. Sagawa, Phys. Rev. C **76**, 047302 (2007).
[21] D. Baye, Phys. Status Solidi B **243**, 1095 (2006).
[22] P. Descouvemont and D. Baye, Rep. Prog. Phys. **73**, 036301 (2010).
[23] E. C. Pinilla, D. Baye, P. Descouvemont, W. Horiuchi, and Y. Suzuki, Nucl. Phys. A **865**, 43 (2011).
[24] H. Esbensen, K. Hagino, P. Mueller, and H. Sagawa, Phys. Rev. C **76**, 024302 (2007).
[25] B. V. Danilin, T. Rogde, J. S. Vaagen, I. J. Thompson, and M. V. Zhukov, Phys. Rev. C **69**, 024609 (2004).
[26] B. V. Danilin, J. S. Vaagen, T. Rogde, S. N. Ershov, I. J. Thompson, and M. V. Zhukov, Phys. Rev. C **73**, 054002 (2006).
[27] D. Baye and P. H. Heenen, J. Phys. A **19**, 2041 (1986).
[28] M. Abramowitz and I. A. Stegun, *Handbook of Mathematical Functions* (Dover, London, 1972).
[29] R. Y. Rasoanaivo and G. H. Rawitscher, Phys. Rev. C **39**, 1709 (1989).
[30] V. I. Kukulin and V. N. Pomerantsev, Ann. Phys. **111**, 330 (1978).
[31] D. Baye, Phys. Rev. Lett. **58**, 2738 (1987).
[32] H. Esbensen, G. F. Bertsch, and K. Hencken, Phys. Rev. C **56**, 3054 (1997).
[33] B. M. Young, W. Benenson, J. H. Kelley, N. A. Orr, R. Pfaff, B. M. Sherrill, M. Steiner, M. Thoennessen, J. S. Winfield, J. A. Winger, S. J. Yennello, and A. Zeller, Phys. Rev. C **49**, 279 (1994).
[34] D. R. Thompson, M. LeMere, and Y. C. Tang, Nucl. Phys. A **286**, 53 (1977).
[35] P. Egelhof *et al*., Eur. Phys. J. A **15**, 27 (2002).
[36] I. Tanihata, T. Kobayashi, O. Yamakawa, S. Shimoura, K. Ekuni, K. Sugimoto, N. Takahashi, T. Shimoda, and H. Sato, Phys. Lett. B **206**, 592 (1988).
[37] A. J. Koning and J. P. Delaroche, Nucl. Phys. A **713**, 231 (2003).

[38] P. Capel, D. Baye, and V. S. Melezhik, Phys. Rev. C **68**, 014612 (2003).
[39] B. Bonin, N. Alamanos, B. Berthier, G. Bruge, H. Faraggi, J. C. Lugol, W. Mittig, L. Papineau, A. I. Yavin, J. Arvieux, L. Farvacque, M. Buenerd, and W. Bauhoff, Nucl. Phys. A **445**, 381 (1985).
[40] S. N. Ershov, B. V. Danilin, J. S. Vaagen, A. A. Korsheninnikov, and I. J. Thompson, Phys. Rev. C **70**, 054608 (2004).
[41] C. Bertulani and G. Baur, Phys. Rep. **163**, 299 (1988).
[42] T. Aumann *et al.*, Phys. Rev. C **59**, 1252 (1999).